# Performance Analysis of Auxiliary Bearing based on Four-contact-point Ball Bearing

Junyu XIA[a], Longxiang XU[a], Chaowu JIN[a], Chengtao YU[b]

[a] College of Mechanical and Electrical Engineering, Nanjing University of Aeronautics and Astronautics, Nanjing 210016, China, nuaaxjy@163.com
[b] Jiangsu University of Technology, 1801 Zhongwu Rd., Changzhou, China, yuct@jsut.edu.cn

***Abstract*—The performance of auxiliary bearings based on four-contact-point ball bearings is studied. Firstly, based on Hertz contact theory, the static model of bearing is established to analyse the influence of structural parameters on stress and strain of the contact part, and the selection range of the optimal parameters is given. Then, the mechanical analysis of four-contact-point ball bearing under different loads is carried out, and the variation law of load distribution is studied by theoretical calculation. Finally, the dynamic model of rotor dropping is established to compare the protection effect between four-contact-point ball bearing and angular contact bearing. A test rig is built to carry out the rotor drop experiment under different bearing protection. The results could be referenced for the design of auxiliary bearings in active magnetic bearing system.**

***Keywords*: auxiliary bearing, active magnetic bearing, four-contact-point ball bearing, rotor drop**

## I. INTRODUCTION[1]

The AMB (active magnetic bearing) system can operate without mechanical contact between rotor and stator through the dynamic control of the electromagnet. Because of its advantages of long service life, low energy consumption, no noise, no pollution, safe and reliable, AMB system has broad application prospects in transportation, machinery, metallurgy, materials, electrical appliances and so on.

In AMB system, the existence of auxiliary bearing is especially important. Its protective effect is mainly reflected in two aspects:

- Provide support for the rotor when the magnetic bearing is in a non-working state;
- During the working process of magnetic bearing, prevent the rotor from colliding with the stator and other parts of magnetic bearing when the bearing is out of control due to accidents.

The diagram of four-contact-point ball bearing is shown in Fig. 1. The race is double circular arc curve, like a peach-shaped groove structure. When under pure radial load or the ratio of axial load to radial load is very small, the ball and raceway are in four-point contact. Compared with conventional two-contact-point ball bearing, the contact deformation is smaller, the bearing capacity is stronger and the limit speed is higher under the same conditions. Compared with the new type of protective bearings, its simple and compact structure can save space and weight.

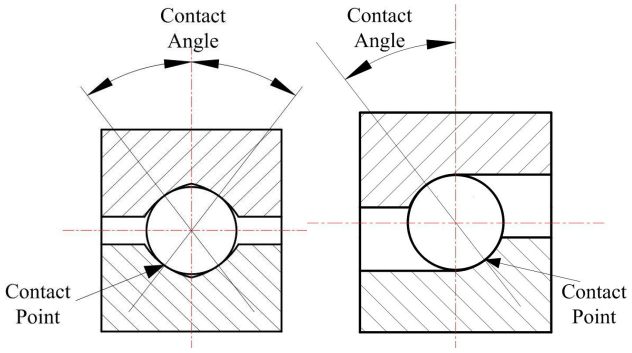


Fig. 1 Four-contact-point ball bearing and angular contact bearing

A lot of research has been carried out on auxiliary bearing and four-contact-point ball bearing. Zhu Changsheng[1],[2] has carried out a series of studies on the process of rotor falling in fixed clearance auxiliary bearings. The effects of the initial fall position, rotor speed, rotor unbalance, support damping and stiffness of bearing are analyzed. Zhu Y *et al.*[3],[4] studies the dynamic response and collision force of the rotor falling on a new type of protective bearing.

PING Lihao *et al.*[5] proves the feasibility of the finite element method for the analysis of the force deformation of four-contact-point ball bearings. ZHU Chunxi *et al.*[6] analyses the contact stress on four-contact-point ball bearing with based on Hertz's contact theory.

However, the application of four-contact-point ball bearing in auxiliary bearing is seldom reported. In this paper, the four-contact-point ball bearing is applied to the auxiliary bearing and the the performance of auxiliary bearings based on four-contact-point ball bearings is studied and compared.

## II. ANALYSIS AND SIMULATION

### A. Theoretical Background

Based on Hertz contact theory, the internal structure of four-contact-point ball bearings is analyzed. The elastic contact problem has the following two basic equations[6]:

Force balance equation:

$$\iint_{A_c} \sigma(x,y)\mathrm{d}x\mathrm{d}y = Q \tag{1}$$

[1] National Nature Science Foundation of China (51605208); Natural Science Foundation of the Jiangsu Higher Education Institutions of China (Grant No.16KJB460008);

Where $A_c$ is the contact area, $\sigma$ is the contact stress, $Q$ is load.

Deformation coordination equation:

$$\frac{1}{\pi E'}\iint_{A_c}\frac{\sigma(x',y')\mathrm{d}x'\mathrm{d}y'}{\sqrt{(x-x')^2+(y-y')^2}}=\delta-z(x,y) \quad (2)$$

$$\frac{1}{E'}=\frac{1-\nu_1^2}{E_1}+\frac{1-\nu_2^2}{E_2} \quad (3)$$

Where $z$ is the initial spacing between two contact bodies, $\delta$ is the elastic approach between the contact bodies, $E$ and $\nu$ are elastic modulus and Poisson's ratio of two bodies.

According to Hertz's point contact theory, the contact region of point contact is an ellipse, then the size of semi-major and semi-minor axis of contact ellipse and the elastic approach can be expressed as:

$$a=a^*\sqrt[3]{\frac{3Q}{2\sum\rho}\left(\frac{1-\nu_1^2}{E_1}+\frac{1-\nu_2^2}{E_2}\right)} \quad (4)$$

$$b=b^*\sqrt[3]{\frac{3Q}{2\sum\rho}\left(\frac{1-\nu_1^2}{E_1}+\frac{1-\nu_2^2}{E_2}\right)} \quad (5)$$

$$\delta=\frac{K(e)}{\pi a^*}\sqrt[3]{\frac{9\sum\rho Q^2}{4}\left(\frac{1-\nu_1^2}{E_1}+\frac{1-\nu_2^2}{E_2}\right)} \quad (6)$$

Where $a^*$ and $b^*$ are semi-major and semi-minor axis coefficients related to curvature function. $\sum\rho$ is curvature sum obtained from the sectional curvature of the contact surface. $K(e)$ is complete elliptic integral of the first kind.

### *B. Contact Analysis*

Suppose GCr15 steel is chosen for balls and 42CrMo steel is chosen for inner and outer ring, $E$ and $\nu$ are $2.07\times10^5$ MPa and 0.3, respectively.

Assuming that the inner and outer race of the bearing are rigid, the deformation occurs at the contact between the ball and the race. Elastic approach can be simplified as:

$$\delta=2.79\times10^{-4}\frac{2K(e)}{\pi a^*}Q^{\frac{2}{3}}\left(\sum\rho\right)^{\frac{1}{3}} \quad (7)$$

Maximum stress:

$$\sigma_0=\frac{3Q}{2\pi ab} \quad (8)$$

Suppose the radial external load $Q$ is 1000N, the stress and strain of steel ball under different structural parameters are calculated.

The initial structural parameters are listed in Table I :

TABLE I. THE INITIAL STRUCTURAL PARAMETERS OF FOUR-CONTACT-POINT BALL BEARING

| | Parameter | Value |
|---|---|---|
| $D_i$ | Inner diameter of bearing inner ring | 15mm |
| $D_o$ | Bearing outer ring diameter | 35mm |
| $D_m$ | Pitch diameter | 25.5mm |
| $d_b$ | Diameter of ball | 6mm |
| $f_i$ | Radius coefficient of inner race | 0.52 |
| $f_o$ | Radius coefficient of outer race | 0.52 |
| $\alpha$ | Initial contact angle | 35° |

Change the contact angle from 10° to 75°, the curve of elastic approach and maximum stress with the change of contact angle can be obtained as shown in Fig. 2(a,b):

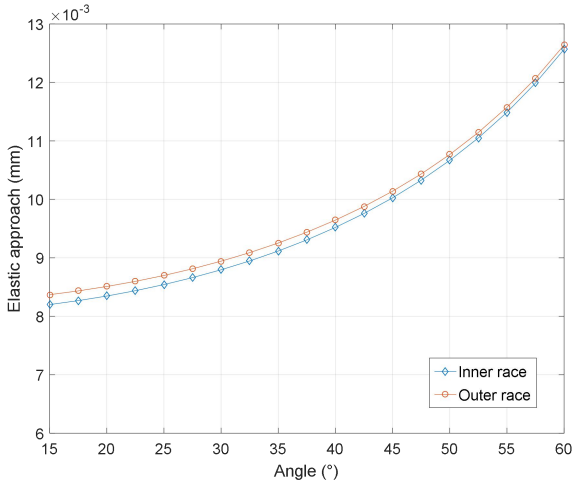


(a)

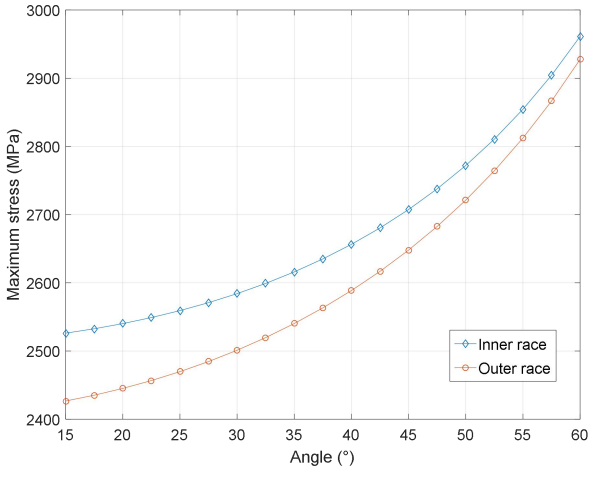


(b)

Fig. 2 (a) Elastic approach and (b) maximum stress of inner and outer race with the change of contact angle

According to the results, it can be found that the maximum stress in inner race is greater than outer race and the elastic approach in inner and outer race are very close to each other.

With the radial load only, elastic approach and the maximum stress at the contact point increases with the increase of contact angle, and the increase is accelerating. It is suggested that reducing the contact angle properly is helpful to improve the radial bearing capacity of four-contact-point ball bearing.

Change the radius coefficient of race from 0.505 to 0.6 to obtain the curve of elastic approach and maximum stress in Fig. 3(a,b):

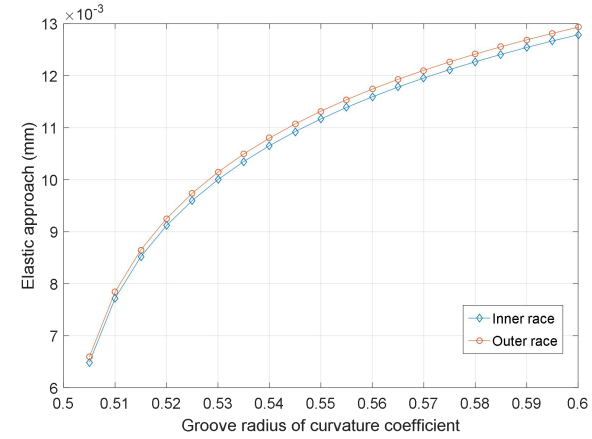


(a)

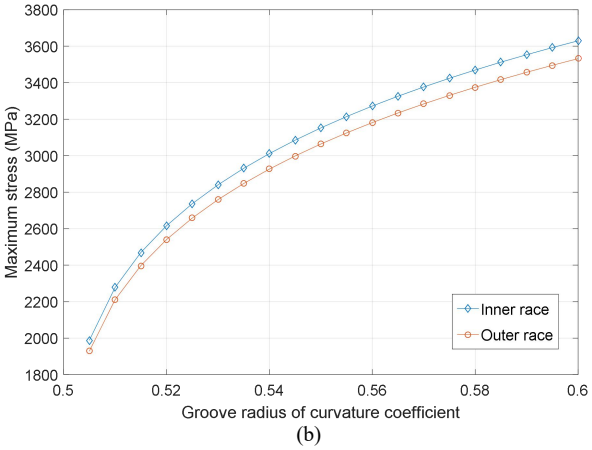


(b)

Fig. 3 (a) Elastic approach and (b) maximum stress of inner and outer race with the change of groove radius of curvature coefficient

The results show that the elastic approach and the maximum stress at contact point increases with the increase of radius coefficient of race, and the increase is slowing down. In order to obtain a better bearing effect, a smaller radius coefficient of race should be selected.

With the initial contact angle of 35° and radius coefficient of 0.52, the model of single ball-channel is established and analyzed by using the finite element software. Fig. 4(a,b) shows the stress distributions of four-contact-point ball bearing and angular contact bearing.

With the same structural parameters, the maximum stress of four-contact-point ball bearing using finite element software is 2346.2MPa, slightly smaller than the theoretical calculated value of 2616MPa, while the maximum stress of angular contact ball bearings is 3043.9MPa. Compared with angular contact bearing, the maximum stress of four-contact-point ball bearing is reduced by 22.9% under the same load, and the bearing effect is better.

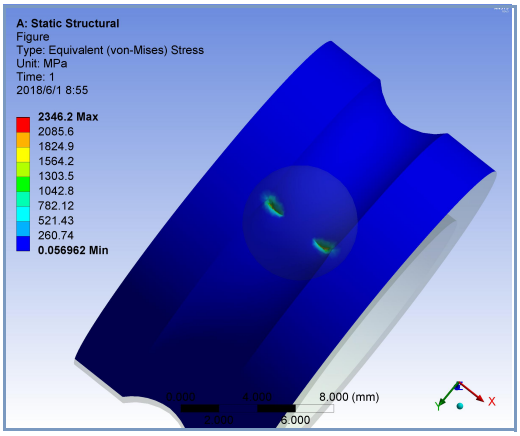


(a)

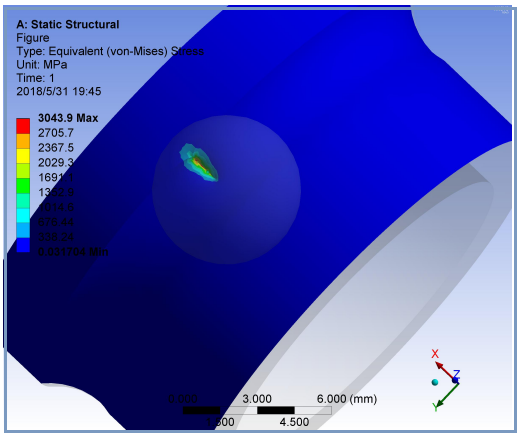


(b)

Fig. 4 The stress distributions of (a) four-contact-point ball bearing and (b) angular contact bearing under 1000N radial load

## C. *Static Analysis*

The bearing parameters are set according to the previous section and the number of balls is set to 11. Under the combined load of radial force, axial force and torque, the deformation of the balls in bearing at different position is shown in Fig. 5:

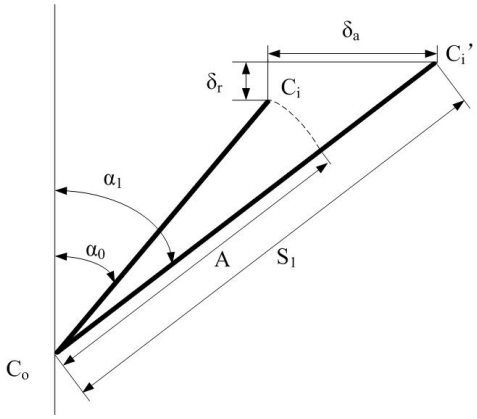


Fig. 5 Geometric deformation of bearing under stress

Where $C_i$ and $C_o$ are the initial center of inner and outer race curvature, respectively. $C_i'$ is the center of inner race curvature under the combined load. The initial central distance $A$ of curvature center of inner and outer ring can be calculated as:

$$A = (f_i + f_o - 1)d_b \tag{9}$$

For four-contact-point ball bearing, two sets of contact pairs are formed on the ball, numbered 1 and 2. The distance $S$ of curvature center of the inner and outer race after loading can be obtained by geometric relation[7]:

$$S_1 = \sqrt{(A\sin\alpha_0 + \delta_a + r_{ic}\theta\cos\phi)^2 + (A\cos\alpha_0 + \delta_r\cos\phi)^2} \tag{10}$$

$$S_2 = \sqrt{(A\sin\alpha_0 - \delta_a - r_{ic}\theta\cos\phi)^2 + (A\cos\alpha_0 + \delta_r\cos\phi)^2} \tag{11}$$

Where $r_{ic}$ is the radius of the central trajectory of the curvature of the inner race, $\phi$ is position angle of balls.

The two pairs of contact angles $\alpha_1$ and $\alpha_2$ after loading satisfy the following formula, respectively:

$$\sin\alpha_1 = \frac{A\sin\alpha_0 + \delta_a + r_{ic}\theta\cos\phi}{\sqrt{(A\sin\alpha_0 + \delta_a + r_{ic}\theta\cos\phi)^2 + (A\cos\alpha_0 + \delta_r\cos\phi)^2}} \tag{12}$$

$$\sin\alpha_2 = \frac{A\sin\alpha_0 - \delta_a - r_{ic}\theta\cos\phi}{\sqrt{(A\sin\alpha_0 - \delta_a - r_{ic}\theta\cos\phi)^2 + (A\cos\alpha_0 + \delta_r\cos\phi)^2}} \tag{13}$$

Accordingly, the static equilibrium equations of the inner ring of the four-contact-point ball bearing under combined load can be set out.

$$\begin{cases} F_a = \sum_{j=1}^{z} K_b(S_1 - A)^{1.5}\sin\alpha_1 - \sum_{j=1}^{z} K_b(S_2 - A)^{1.5}\sin\alpha_2 \\ F_r = \sum_{j=1}^{z} K_b(S_1 - A)^{1.5}\cos\alpha_1\cos\phi_j + \sum_{j=1}^{z} K_b(S_2 - A)^{1.5}\cos\alpha_2\cos\phi_j \\ M = 0.5 d_m K_b\left(\sum_{j=1}^{z}(S_1 - A)^{1.5}\sin\alpha_1\cos\phi_j - \sum_{j=1}^{z}(S_2 - A)^{1.5}\sin\alpha_2\cos\phi_j\right) \end{cases} \tag{14}$$

Where $K_b$ is total contact stiffness of the ball bearing, $K_i$ and $K_o$ are stiffness coefficients of inner and outer race

$$K_b = \frac{K_i K_o}{\left(K_i^{\frac{2}{3}} + K_o^{\frac{2}{3}}\right)^{-\frac{3}{2}}} \tag{15}$$

Solving Eq.(14) by Newton-Raphson method, the load distribution of ball and the influence of external load on internal structural parameters of steel ball can be found.

Fig. 6(a,b,c,d) shows that radial load causes contact angle to change along the position angle, and the greater the radial load, the greater the difference of contact angle. With the increase of axial load, contact angle of the corresponding direction increases and another direction decreases.

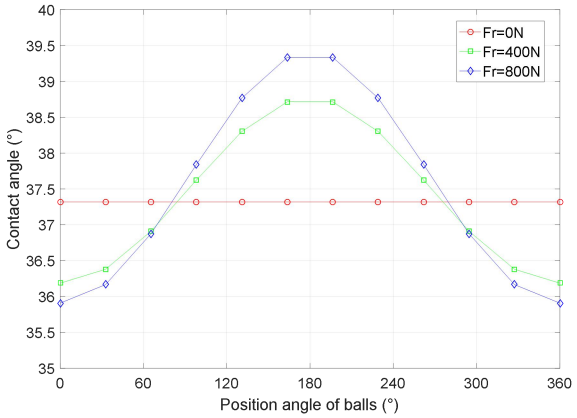

(a) Axial force is 1000N

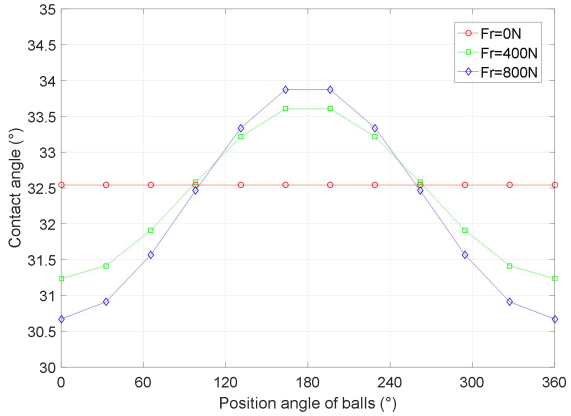

(b) Axial force is 1000N

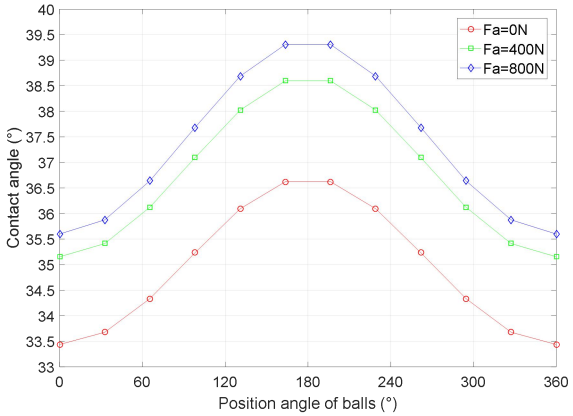

(c) Radial force is 1000N

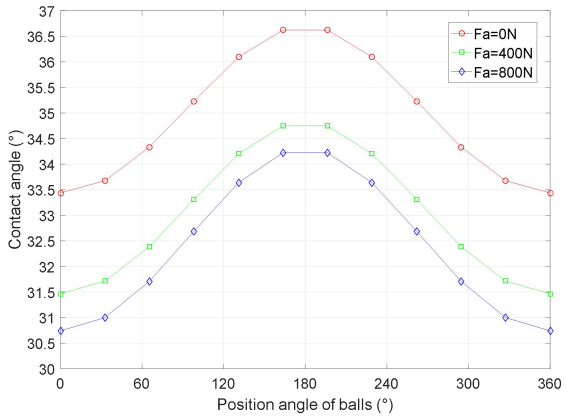


(d) Radial force is 1000N

Fig. 6 Distribution of contact angle with the change of axial and radial force. (a) (c) are contact pair1 and (b) (d) are contact pair2

The influence of external load on axial and radial displacement of bearing is shown in Fig. 7(a,b). It can be seen that with the increase of the load in one direction (radial or axial), the displacement in this direction increases obviously, and the displacement in the other direction (axial or radial) increases slightly.

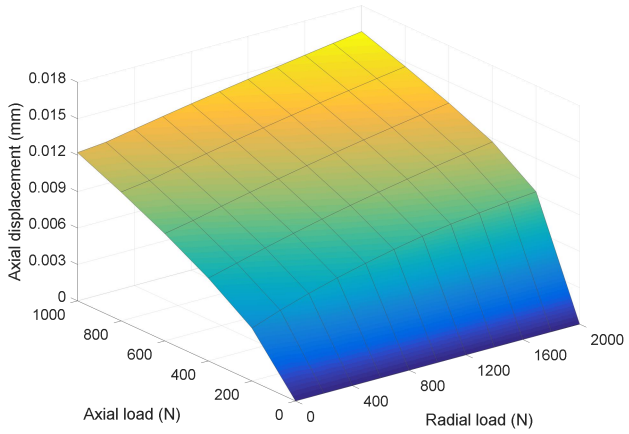


(a)

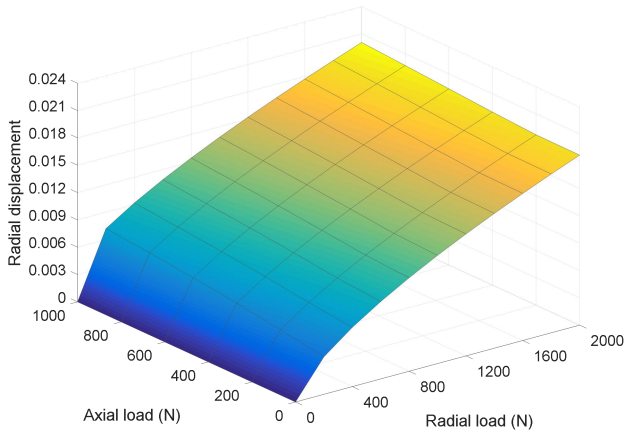


(b)

Fig. 7 (a) Axial displacement and (b) radial displacement with the change of axial and radial load

The analysis method for angular contact bearing is similar to the above, and the static equilibrium equation of the inner ring can be expressed as follows:

$$\begin{cases} F_a = \sum_{j=1}^{z} K_b \left(S_1 - A\right)^{1.5} \sin\alpha_1 \\ F_r = \sum_{j=1}^{z} K_b \left(S_1 - A\right)^{1.5} \cos\alpha_1 \cos\phi_j \\ M = 0.5 d_m K_b \sum_{j=1}^{z} \left(S_1 - A\right)^{1.5} \sin\alpha_1 \cos\phi_j \end{cases} \tag{16}$$

The maximum stress of four-point contact ball bearing and angular contact bearing under radial load is obtained:

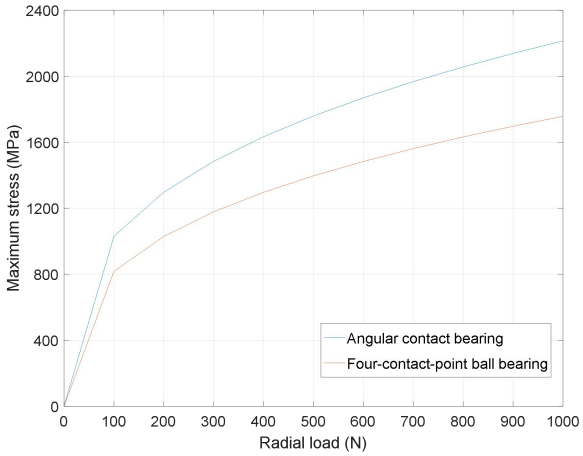


Fig. 8 The maximum stress of different bearings under radial load

With the increase of radial load, the maximum stress of the bearing increases first quickly and then slowly. The maximum stress of the angular contact bearing is greater than that of the four-point contact ball bearing, and the excess value increases continuously.

## *D. Drop Analysis*

The rotor motion state is analyzed by establishing the dynamic model of rotor dropping on the auxiliary bearing.

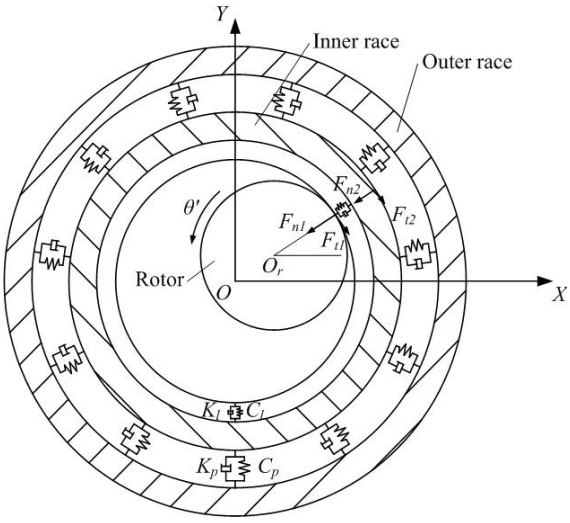


Fig. 9 Diagram of rotor drop

Fig. 9 shows the rotor drop diagram. Suppose the rotor falls from the center, the rotor radius is $r$, the single side clearance is $s$. The depth of the rotor immersed in the bearing inner ring can be expressed as:

$$\delta_r = \sqrt{(x_r - x_b)^2 + (y_r - y_b)^2} - s \tag{17}$$

Relative compression deformation between bearing inner ring and ball:

$$\delta_b = \sqrt{x_b^{\ 2} + y_b^{\ 2}} \tag{18}$$

When the rotor is in contact with the inner ring of the bearing, the bearing plays a protective role. In this case, the rotor is subjected to the normal contact force and tangential friction from the inner ring of the bearing.

Expression of normal contact force can be derived as:

$$F_{n1} = K_l \delta^{10/9} + C_l V_{n1} \tag{19}$$

$$V_{n1} = \frac{(\dot{x}_r - \dot{x}_b)(x_r - x_b) + (\dot{y}_r - \dot{y}_b)(y_r - y_b)}{\sqrt{(x_r - x_b)^2 + (y_r - y_b)^2}} \tag{20}$$

Where $K_l$ is the contact stiffness calculated by Hertz line contact theory. Tangential force can be calculated based on Coulomb friction:

$$F_{t1} = \mu_1 F_{n1} \tag{21}$$

When the bearing inner ring is displaced by collision, the expression of axial load is given by Ref. [8]:

$$F_r = \sum_{j=1}^{Z} K_b \delta_{\phi_j}^{\frac{3}{2}} \cos \phi_j \tag{22}$$

The normal force $F_{n2}$ and tangential force $F_{t2}$ of the bearing inner ring can be expressed as:

$$F_{n2} = F_r + C_b \dot{\delta}_b \tag{23}$$

$$F_{t2} = \mu_2 F_{n2} \tag{24}$$

The dynamic equations of the rotor and inner race can be obtained:

$$\begin{cases} m_r \ddot{x}_r = -F_{n1} \cos \beta_1 + F_{t1} \sin \beta_1 + \dot{\theta}_r^{\ 2} e m_r \cos \theta_r \\ m_r \ddot{y}_r = -F_{n1} \sin \beta_1 - F_{t1} \cos \beta_1 + \dot{\theta}_r^{\ 2} e m_r \sin \theta_r - m_r g \\ J_r \ddot{\theta}_r = -F_{t1}[r - e\cos(\beta_1 - \theta_r)] + F_{n1} e \sin(\beta_1 - \theta_r) - m_r e g \cos \theta_r \end{cases} \tag{25}$$

$$\begin{cases} m_b \ddot{x}_b = F_{n1} \cos \beta_1 - F_{t1} \sin \beta_1 - F_{n2} \cos \beta_2 + F_{t2} \sin \beta_2 \\ m_b \ddot{y}_b = F_{n1} \sin \beta_1 + F_{t1} \cos \beta_1 - F_{n2} \cos \beta_2 - F_{t2} \sin \beta_2 - m_b g \\ J_b \ddot{\theta}_b = (F_{t1} - F_{t2})(s + r) \end{cases} \tag{26}$$

Where $\beta_1 = \arctan\left(\frac{y_b - y_r}{x_b - x_r}\right)$, $\beta_2 = \arctan\left(\frac{y_b}{x_b}\right)$.

When $\delta_r \le 0$, there is no contact between rotor and bearing inner race, $F_{n1} = F_{t1} = 0$.

Assume that the rotor drops with the speed of 6000 rpm, the initial conditions for the system are set to:

$$\begin{aligned} &\left(\mathrm{x_r}, \dot{\mathrm{x}}_\mathrm{r}, \mathrm{y_r}, \dot{\mathrm{y}}_\mathrm{r}, \theta_\mathrm{r}, \dot{\theta}_\mathrm{r}, \mathrm{x_b}, \dot{\mathrm{x}}_\mathrm{b}, \mathrm{y_b}, \dot{\mathrm{y}}_\mathrm{b}, \theta_\mathrm{b}, \dot{\theta}_\mathrm{b}\right) \\ &= (0,0,0,0,0,628,0,0,0,0,0,0) \end{aligned}$$

The numerical solutions can be solved using Runge-Kutta algorithm. The total integration time is 0.15s and time step is 0.0001s. By solving the differential equations above, dynamic responses of the rotor's touchdowns after AMB system failure can be simulated and the data of orbit response, collision force, angular velocity and so on can be obtained.

The main parameters of the rotor-bearing system are listed in Table II and the orbit responses and collision force of dropping process are shown in Fig. 10(a,b) and Fig. 11(a,b).

TABLE II. PARAMETERS OF ROTOR-BEARING SYSTEM

| | Parameter | Value |
|---|---|---|
| $m_r$ | Mass of rotor | 1.48kg |
| $J_r$ | Polar MOI of rotor | $3.88\times10^{-4}\,\mathrm{kg\cdot m^2}$ |
| $m_b$ | Mass of inner race | 0.0125kg |
| $J_b$ | Polar MOI of rotor | $7.03\times10^{-7}\,\mathrm{kg\cdot m^2}$ |
| $Z$ | Number of balls | 11 |
| $e$ | Imbalance eccentricity of rotor | $1\times10^{-5}\,\mathrm{m}$ |
| $K_l$ | Stiffness coefficient of line contact | $1.468\times10^{9}\,\mathrm{N\cdot m^{-10/9}}$ |
| $C_l$ | Damping coefficient of line contact | $1000\,\mathrm{N\cdot s\cdot m^{-1}}$ |
| $K_b$ | Stiffness coefficient of point contact | $5.42\times10^{5}\,\mathrm{N\cdot m^{-1.5}}$ |
| $C_b$ | Damping coefficient of point contact | $500\,\mathrm{N\cdot s\cdot m^{-1}}$ |
| $\mu_1$ | Sliding friction coefficient | 0.2 |
| $\mu_2$ | Rolling friction coefficient | 0.01 |

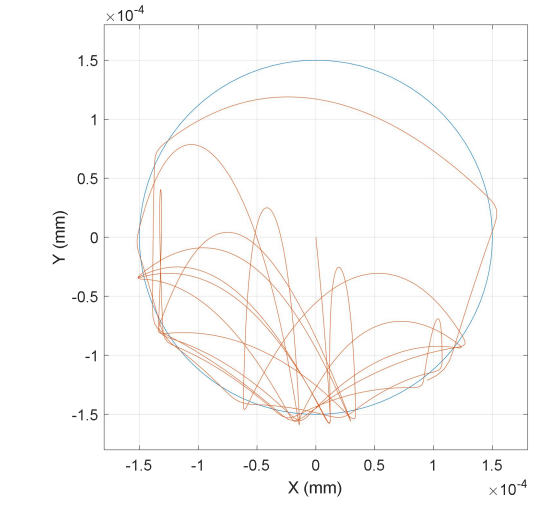


(a)

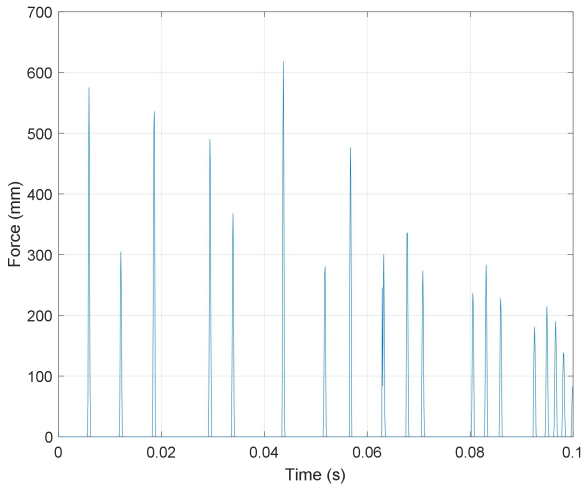


(b)

Fig. 10 (a) Orbit response and (b) collision force during rotor dropping on four-contact-point ball bearing

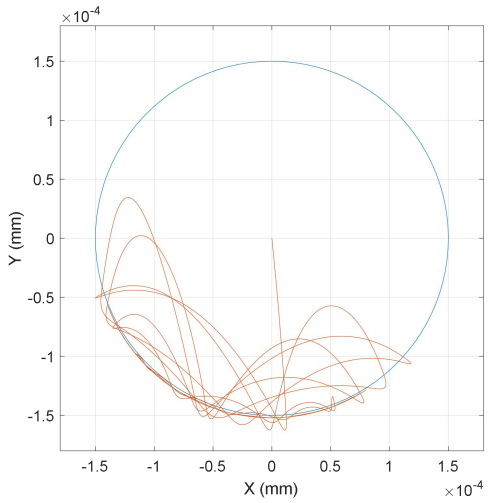


(a)

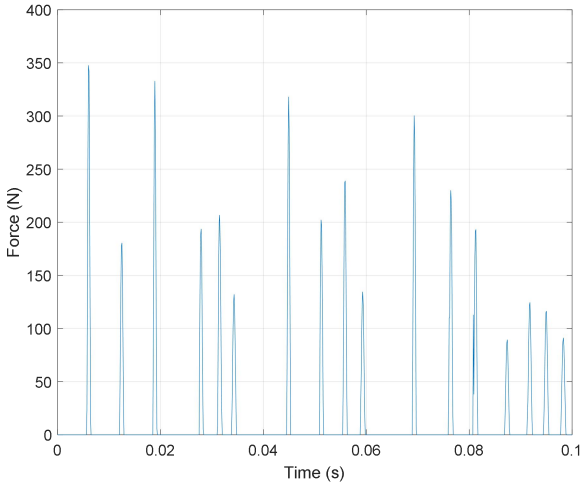


(b)

Fig. 11 (a) Orbit response and (b) collision force during rotor dropping on angular contact bearing

According to the simulation results, the rotor behaves like combined rub and bouncing during dropping process. When rotor drops on the auxiliary bearing based on four-contact-point ball bearing, it has a tendency to backward whirl.

By analyzing the collision force, it can be found that under the protection of angular contact bearings, the maximum collision force during drop is 391N, and the maximum internal stress is 1634MPa. Under the protection of four-contact-point ball bearing, the maximum collision force of 618N is about 1.58 times that of angular contact bearing. However, the maximum stress of 1483MPa in the bearing decreases by 10.2% compared with angular contact ball bearing.

## III. EXPERIMENT

In order to study the motion state of rotor after dropping, a test rig is built to carry out the rotor drop experiment. The experimental facilities necessary for measurement are shown in Fig. 12.

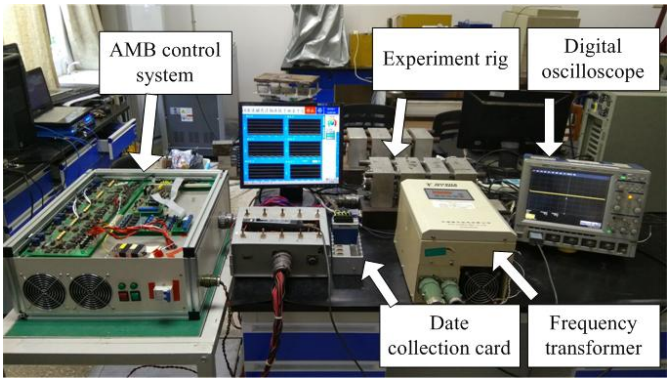


Fig. 12 Photograph of experimental facilities

QJ202 and 7202 bearings are used as auxiliary bearing, respectively. In the experiment, the rotor is first suspended and rotated at a fixed speed of 6000rpm, then the power supply of the AMB system is cut off by drop control switch, the rotor falls and collides with the inner ring of the bearing, and the orbit response is recorded.

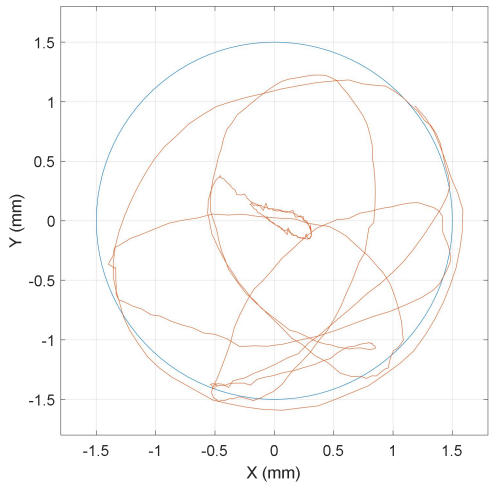


(a)

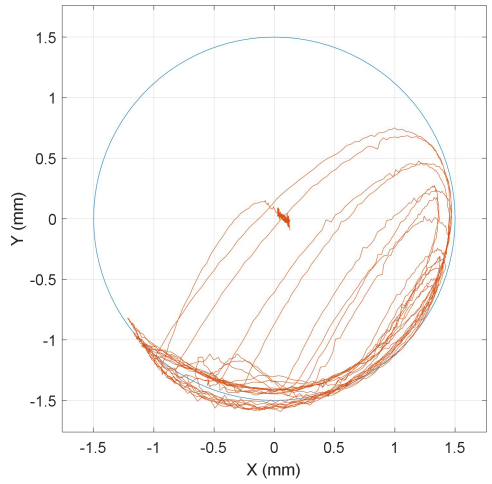


(b)

Fig. 13 Orbit response during rotor dropping on (a) four-contact-point ball bearing and (b) angular contact bearing

During the experiment, the rotor only collides with the auxiliary bearing, and there is no bearing damage. Combined with the experimental results, the maximum stress in the collision process is calculated.

Under the protection of four-contact-point ball bearing, the maximum stress of 1728MPa is close to the simulation result of 1483MPa while the maximum stress of 2348MPa in angular contact bearing has big difference. The main reasons are as follows:

- The parameters of 7202 bearings used in experiment are different from simulation. For example, the contact angle is 40° instead of 35°.
- Different angle of imbalance eccentricity at the moment of dropping causes different orbit responses.
- The theoretical model is based on many assumptions and cannot be identical to the actual model.
- Measurement error.

However, the results of experiment and simulation are coincident that the maximum stress of four-point contact ball bearing is smaller than that of angular contact bearing.

## IV. CONCLUSIONS

In this paper, the performance of auxiliary bearings based on four-contact-point ball bearings is studied. A static model of bearing is established to obtain the selection range of the optimal structural parameters. The dynamic responses of the rotor drops on four-contact-point ball bearing and angular contact bearing are respectively simulated. Finally, rotor drop experiments are carried out to compare the protection effect between four-contact-point ball bearing and angular contact bearing. The following conclusions can be obtained:

- Reducing the contact angle and radius coefficient of race properly is helpful to reduce the elastic approach and stress, thus, improve the radial bearing capacity of four-contact-point ball bearing. The recommended contact angle is 15-45, and the recommended radius is 0.51-0.52.
- Axial load changes the contact angle, and radial load on four-contact-point ball bearing causes the ball contact angle to change along the position angle. With the increase of the load in one direction (radial or axial), the displacement in this direction increases obviously, and the displacement in the other direction (axial or radial) increases slightly.
- Compared with the protection of angular contact bearing, the maximum collision force and bounce amplitudes of four-contact-point ball bearing is bigger. However, the maximum stress in four-contact-point ball bearing decreases compared with the angular contact ball bearing.

## REFERENCES

[1] Zhu changsheng, Nonlinear Dynamics of Rotor Drop on Rolling Element Backu Bearings After Active Magnetic Bearings Failure[J]. Journal of Mechanical Engineering, 2006, 42(7):196-202.

[2] Zhu changsheng, Experimental Investigation into the Transient Response of a Flexible Rotor Dropping on a Back-up Bearing After Active Magnetic Bearings Failure[J]. Acta Aeronautica ET Astronautica Sinica, 2009, 30(8):1537-1543.

[3] Zhu Y, Jin C, Longxiang XU. Dynamic Responses of Rotor Drops onto Double-decker Catcher Bearing[J]. Chinese Journal of Mechanical Engineering, 2013, 26(1):104-113.

[4] Zhu Y, Jin C. Maximum Impact Force and Thermal Characteristic Analysis of Double-decker Catcher Bearing Used in High-speed and Heavy-load Conditions[J]. China Mechanical Engineering, 2016, 27(1):25-31.

[5] PING Lihao, WANG Changwu, LI Liangjun. Contact Problems of Gothic-arc Bearing[J]. Journal of Nanjing University of Science and Technology, 2007, 31(4):458-461.

[6] ZHU Chunxi, WANG Guohua, ZONG Chunli, CHENG Guangwei. Contact Stress Analysis on Large-sized Four-contact-point Ball Bearing with Negative Internal Clearance Based on Hertz's Contact Theory[J]. Manufacturing Technology & Machine Tool, 2011(2):139-141.

[7] JI Yonggang, WANG Yanshuang. Calculation of Static Stiffness of Four-contact-point Ball Bearing[J]. Journal of Henan University of Science and Technology(Natural Science), 2013, 34(2):22-25.

[8] Lyu M, Wang Z, Liu T, et al. Frequency Analysis of the Orbit Responses of Active Magnetic Bearings in Touchdown Using Hilbert Transform[J]. International Journal of Structural Stability & Dynamics, 2016, 17(8):1750086.